Magneto-optical Kerr spectra of gold induced by spin accumulation

Víctor H. Ortiz ⓞ, Sinisa Coh,* and Richard B. Wilson ⓞ†

Department of Mechanical Engineering and Materials Science and Engineering Program,
University of California, Riverside, California 92521, USA

We report the magneto-optic Kerr effect (MOKE) angle of Au magnetically excited by spin accumulation. We perform time-resolved polar MOKE measurements on Au/Co heterostructures. In our experiment, the ultrafast optical excitation of the Co drives spin accumulation into an adjacent Au layer. The spin accumulation, together with spin-orbit coupling, leads to nonzero terms in the off-diagonal conductivity tensor of Au, which we measure by recording the polarization and ellipticity of light reflected from the Au surface for photon energies between 1.3 and 3.1 eV. In a narrow energy range near the interband transition threshold of Au, the sensitivity to magnetization measured exceeds 1 μrad per A/m. In the photon energy interval of 0.6–4.4 eV, the maximum value for transition ferromagnetic metals like Ni are <10 nrad per A/m, while predicted values for heavy metals like Pt or W are <13 nrad per A/m. The exceptional sensitivity of the optical properties of Au to spin magnetic moments make Au an exceptionally sensitive optical magnetometer, with potential applications in the development of optospintronic technologies.

I. INTRODUCTION

Spin-orbit interactions affect how the electrons of a metal move in response to electromagnetic fields [1]. The effect of spin-orbit interactions on motion is opposite for up vs down electrons. In magnetic metals, where the number density of up vs down spins is different, spin-orbit interactions give rise to the well-known magneto-optic Kerr and Faraday effects [2]. These magneto-optic effects describe how the polarization of reflected or transmitted electromagnetic waves differs from the incident wave. Alternatively, in nonmagnetic metals, the net effect spin-orbit interactions on optical properties is zero. This is because, in their ground state, nonmagnetic metals have equal number densities of up vs down spins.

In the presence of an external magnetic field, nonmagnetic metals display magneto-optic effects for two reasons. First, the static magnetic field applies a Lorentz force, which affects the motion of the electrons and gives rise to nonzero off-diagonal terms in the optical conductivity tensor [3]. Second, applying a magnetic field to a metal leads to Zeeman splitting, i.e., leads to spin- and orbital magnetic moments [4]. The direct effect of the Lorentz force exerted by the static magnetic field on the optical properties of a metal is analogous to the Hall effect [3], while the combined effect of spin-accumulation and spin-orbit interactions on the optical properties is analogous to the anomalous Hall effect [5]. Numerous experimental and theoretical studies have documented the magneto-optical properties of nonmagnetic metals in the presence of a static magnetic field [4,6–8]. Alternatively, the physics of how only spin accumulation induces magneto-optical properties in the absence of orbital moments or Lorentz fields is not well understood. Prior experimental studies of spin-accumulation induced magneto-optic Kerr effect (MOKE) in nonmagnetic metals were limited to a single photon energy [5,9]. No prior experimental studies of spin-accumulation induced MOKE have reported spectra across a wide energy range.

Understanding how only spin-accumulation and spin-orbit interactions affect the optical properties of nonmagnetic metals is important for a number of emerging fields. MOKE signals from nonmagnetic metals allow experimentalists to measure a number of spin-transport material properties. Stamm *et al.* used MOKE signals to measure the spin-Hall conductivity and spin-diffusion length of Pt and W [10]. Melnikov *et al.* used time-resolved measurements of nonlinear magneto-optic properties to characterize spin-polarized hot carrier transport in Fe/Au bilayers [9]. Time-resolved MOKE signals from nonmagnetic metals allows for the measurement of spin caloritronic transport properties of adjacent magnetic materials [5,11–13]. Hofherr *et al.* used time-resolved measurements of the complex Kerr effect from Au/Ni bilayers to separately measure the ultrafast magnetization dynamics of both layers [14].

Magnetoplasmonics is another field of study where understanding how spin-orbit interactions affect optical properties is critical [15–23]. The ability of plasmonic resonances to enhance magneto-optical effects such as the inverse Faraday effect has received significant recent attention [19,20,23–26]. The inverse Faraday effect describes the ability of circularly polarized light to induce a magnetic moment in a metal [24,25]. Interpretation of MOKE signals that arise from the inverse Faraday effect (IFE) is challenging, because the magnetic moment induced by IFE can include both orbital and spin contributions [27].

In this work, we report experimental measurements of the complex Kerr spectra of Au in the presence of spin accumulation. We perform a series of time-resolved magneto-optic

---

*Corresponding author: sinisa@ucr.edu
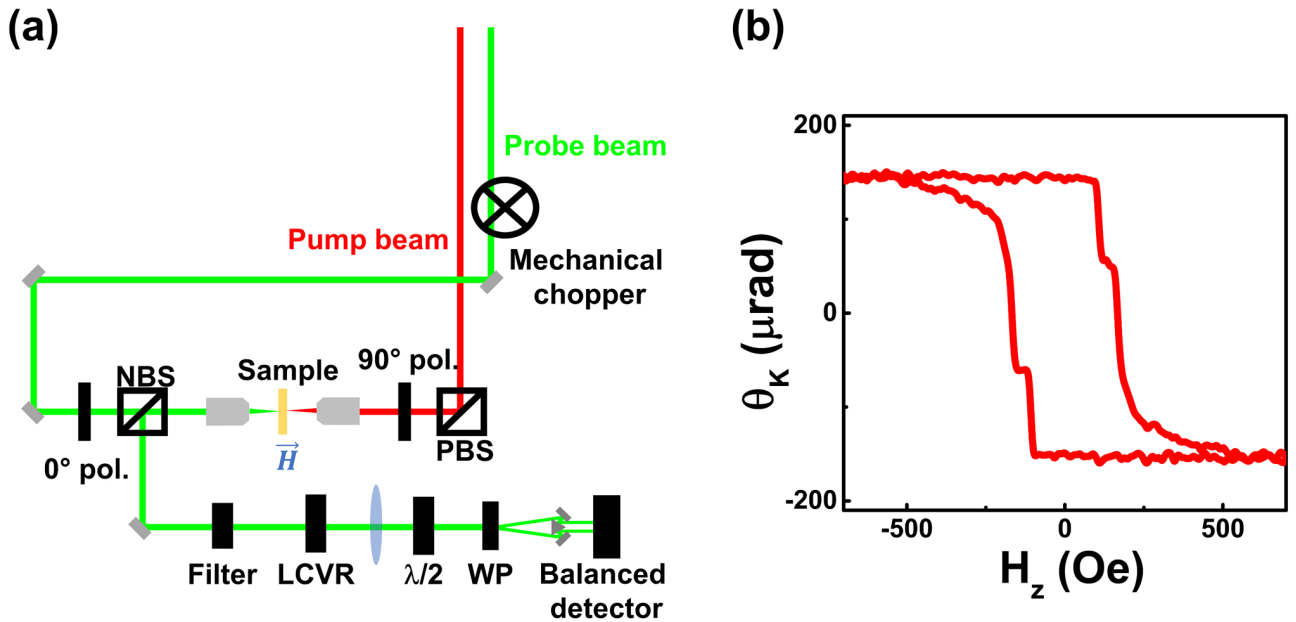†Corresponding author: rwilson@ucr.edu

(a)

(b)

FIG. 1. Experimental setup. (a) Schematic of the pump/probe experiments. The pump beam heats up the sample, causing the spin injection into the Au layer, the reflected probe beam goes through a filter to eliminate any leaked possible pump beam, then through the liquid crystal variable retarder (LCVR), the half-wave plate ($\lambda/2$), and the Wollaston prism (WP). (b) Magnetic field-dependent polar magneto-optic Kerr effect of the Au/Co multilayer.

Kerr effect (TR-MOKE) measurements of a Au/Co multilayer as a function of laser energy. Our experiments span photon energies between 1.3 and 3.1 eV. We observe a resonance-like behavior in the Kerr spectra of Au near an interband transition threshold energy of 2.5 eV. The Kerr angle of Au is $\sim$20$\times$ larger at energies near the interband transition threshold then in the near infrared. On a sensitivity basis, given by the Kerr rotation per magnetic moment, we find that the Kerr angle of Au near 2.5 eV is $\sim$100$\times$ greater than the maximum in visible spectral range in ferromagnetic metals like Ni [28]. To our knowledge, the only material with a comparable magneto-optical response per moment is antiferromagnetic metal Mn_3Sn, whose large Kerr effect origin relates to ferroic ordering of magnetic octupoles [29].

We also performed density-functional theory predictions of the MOKE spectra of gold. Our theory includes the intrinsic effects of spin-orbit interactions on the band structure. The theory neglects spin-orbit scattering effects like side-jump scattering and skew scattering. We also neglect the effect of surfaces, so any effects from spin-orbit induced spin splitting of surface-state bands are not included in our predictions [30]. Overall, the agreement between theory and experiment is excellent, suggesting intrinsic band-structure effects adequately explain the magnitude of observed MOKE signals.

II. EXPERIMENTAL METHODS

A. Sample preparation

We grew the metal multilayer on a (0001)-oriented Al_2O_3 substrate (MTI Corporation). The substrate was thoroughly cleaned and annealed at 1100 °C in air for 1 h to improve surface quality. After annealing, we deposited a 4-nm Ta/4-nm Au/(1-nm Co/2-nm Au) $\times$ 4 multilayer using an AJA Orion sputtering system, in a 3.5-mTorr Ar atmosphere with a power

of 200 W. The sample stage was rotated during deposition at 20 rpm. After deposition of the Au/Co multilayer, we annealed *in situ* at 250 °C for 30 min to sharpen the multilayer interfaces. After cooling down back to room temperature, we stopped the stage rotation, and, without breaking the vacuum, we rotated a metal shutter to partially cover the substrate. The spacing between the shutter and sample was $\sim$5 mm. We then sputter deposited a thick Au layer. The shutter shadows part of the substrate from Au deposition and causes the Au layer to have a thickness gradient (wedge layer), with a thickness between 0 and 300 nm.

B. Pump/probe measurements

We performed time-domain thermoreflectance (TDTR) and TR-MOKE experiments on our sample using a pump-probe system built around a Mai-Tai Ti:sapphire laser with a repetition rate of 80 MHz, and wavelength tunable between 700 and 1050 nm. A lithium triborate crystal serves as a second-harmonic generator to extend the wavelength range of the probe beam to 400 to 525 nm. A schematic of the experimental setup is shown in Fig. 1(a). For the different used wavelengths, the pump-beam spot size ranges from 8.3 to 9.3 μm. The probe-beam spot size ranges from 8.3 to 9.3 μm in the 1.3–1.7-eV photon energy interval, and from 5.4 to 6.8 μm in the 2.4–3.1-eV interval. The pulse duration goes from 80 to 160 fs. Further details of our pump/probe apparatus are reported in Gomez *et al.* [31]. The pump beam impinges on the sample through the sapphire substrate and is absorbed by the metallic multilayer sample. The probe beam reflects from the Au surface at the opposite side of the metal multilayer. The reflected probe beam is then directed towards a detection line so that pump-induced changes in the polarization of the reflected probe beam can be

measured. The detection line includes a beam splitter (Newport 10BC17MB.1 and 10BC17MB.2), liquid-crystal variable retarder (LCVR) (Thorlabs LCC1423-A and LCC1423-B), superachromatic half-wave plate (Thorlabs SAHWP05M-700), Wollaston prism (Newport 10WLP08), and balanced photodetector (Thorlabs PDB450C); see Fig. 1(a). We carefully aligned the beam with a series of apertures to ensure either normal or 45° angle of incidence with all optical elements. We found even slight misalignments of a few degrees hindered our ability to accurately measure real vs imaginary Kerr signals. This sensitivity to alignment is likely due to the dependence of the phase of the laser beam on the angle of incidence with certain optical elements, e.g., the wave plate, optical filters, and beam splitter.

The LCVR allows us to compensate for ellipticity introduced to the probe beam by the detection line reflecting elements (beam splitter and mirror). We calibrate the retardance of the LCVR by placing a 45° polarizer upstream of the optical elements to be compensated (in this case, a beam splitter and mirror). We measure the polarization state of the beam immediately after the LCVR with either a visible or near-infrared polarimeter (Thorlabs PAX 1000). By adjusting the voltage of the LCVR, we control the net retardance caused by the detection line optical elements and LCVR. For measurements of the real part of the Kerr angle (ellipticity $\varepsilon = 0$), we set the net retardance to zero by adjusting the voltage until the probe beam is linearly polarized after the LCVR. For measurements of the imaginary part of the Kerr angle, the net retardance is set to $\lambda/4$ by adjusting the LCVR voltage until the probe beam is circularly polarized. After the proper LCVR voltages are determined for that particular laser wavelength, we remove the 45° polarizer prior to performing pump/probe measurements of the Au multilayer. The above process was repeated at each wavelength we studied, i.e., 16 times.

During pump/probe measurements, we applied an external magnetic field of $\sim\pm2$ kOe on the sample. The 2-kOe field is enough to saturate the magnetic moment of the Au/Co multilayer in the out-of-plane direction; see the MOKE measurement of the hysteresis loop in Fig. 1(b). We orient the half-wave plate before the Wollaston prism until there is equal intensity on both inputs of the balanced photodetector. Then, the voltage output of the balanced photodetector is proportional to the change in polarization caused by the Au. For TDTR measurements, we block one of the inputs of the balanced photodiode. Then, the voltage output by the detector is proportional to the change in reflected intensity.

III. RESULTS

A. Theory

We use the first-principles calculated electron band structure energies E_{nk} and orbitals ψ_{nk} within the perturbative approach to evaluate the optical conductivity of Au [32,33],

$$\sigma_{\alpha\beta}(\omega) = \frac{i\,e^2\hbar}{(2\pi)^3} \lim_{q\to 0} \int dk$$
$$\times \sum_{n,m} \frac{f_{mk+q} - f_{nk}}{E_{mk+q} - E_{nk}} \frac{\langle\psi_{nk}|v_\alpha|\psi_{mk+q}\rangle \langle\psi_{mk+q}|v_\beta|\psi_{nk}\rangle}{E_{mk+q} - E_{nk} - \hbar\omega - i\eta_{mnk}/2}.$$
(1)

The conductivity $\sigma_{\alpha\beta}$ describes the current in direction α in response to electric field pointing in direction β. Equation (1) is a summation over possible electronic transitions between states in band m at wave vector $k + q$ to states in band n and wave vector k. The limit $q \to 0$ indicates that we include here both intraband and interband contributions to the optical conductivity. We take the $q \to 0$ limit analytically using the Wannier interpolation technique as implemented in WANNIER90. The Fermi-Dirac distribution occupation factor is denoted as f while velocity operator is v. η_{mnk} describes the effect of electronic scattering rates on transitions due to electron scattering. We model η_{mnk} with spin-independent electron-electron and electron-phonon scattering which reproduces both first-principles calculations [34]. We also add to η_{mnk} constant spin-independent extrinsic scattering of 0.1 eV to correctly reproduce the imaginary part of the diagonal component of the conductivity tensor (Supplemental Material [35]). We find that the extrinsic scattering modifies Kerr effect mostly via the changes in the imaginary part of the diagonal component of the conductivity tensor. There is nearly no change in the off-diagonal conductivity due to the extrinsic part of the scattering.

We calculate electron wave functions and energies using the Perdew-Burke-Ernzerhof exchange-correlation functional for solids with Hubbard U parameter (PBEsol+U) approach as implemented in the QUANTUM ESPRESSO package [36]. We use $U = 2.7$ eV following Brown *et al.* [37]. We sample the charge density on a $12\times12\times12$ mesh of k points in the equivalent one-atom unit cell. We use Wannier interpolation to converge the optical conductivity on a $300\times300\times300$ mesh of k points.

From the computed diagonal and off-diagonal optical conductivity, we calculate the complex Kerr angle. In the polar MOKE configuration ($\hat{z}$ perpendicular to the sample plane), the complex Kerr angle is

$$\theta_k(\omega) + i\varepsilon_k(\omega) = \frac{\sigma_{yx}(\omega)}{\sigma_{xx}(\omega)\sqrt{1 + i\frac{\sigma_{xx}(\omega)}{\omega\epsilon_0}}}.$$
(2)

Here, θ_k is the Kerr rotation and ε_k is the ellipticity. θ_k describes rotation of the major axis of polarization and is caused by differences in the indices of refraction for left vs right circularly polarized light. ε_k describes a change in the ellipticity and is caused by differences in absorption for left vs right circularly polarized light.

B. Time-resolved magneto-optical Kerr effect experiment

To measure the magneto-optical spectra of Au, we use ultrafast demagnetization of an adjacent ferromagnetic layer to temporarily magnetize the Au film without any external magnetic field. We utilize a Au/Co multilayer system as the ferromagnetic layer with perpendicular magnetic anisotropy [Fig. 1(b)] [38]. The sample geometry is d_{Au}Au/[1-nm Co/2-nm Au]$_{x4}$/2-nm Au/4-nm Ta/sapphire. The top gold film is a wedge layer, with varied thickness d_{Au} between 0 and 300 nm. In our pump/probe experiments, the pump beam causes an increase in the temperature of the Au/Co ferromagnetic multilayer, resulting in ultrafast demagnetization of the Au/Co multilayer [39]. Ultrafast
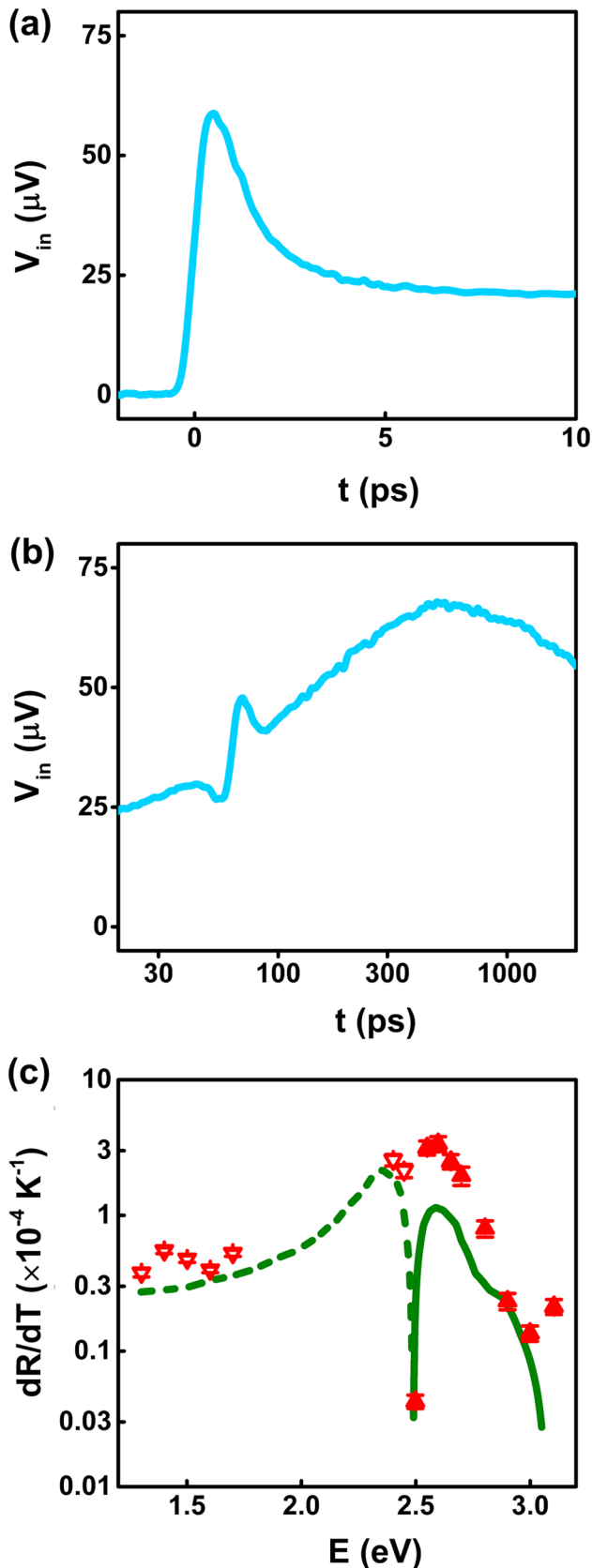
FIG. 2. Time-domain thermoreflectance (TDTR) measurements. (a) In-phase voltage signal vs delay time for a probe energy $E = 2.60$ eV. Experimental signals are caused by temperature-induced changes to the reflectance of the Au. At picosecond timescales, the experimental signals reflect energy transport by hot electrons.

demagnetization of the Au/Co multilayer leads to an injection of spin current in adjacent nonmagnetic layers [5,11]. Spin accumulation in the Au layer causes a rotation of the polarization state of a time-delayed reflected probe beam.

Following pump heating of the Au/Co multilayer, we observe transient changes in the Au reflectance. In Fig. 2, we show TDTR data taken with pump and probe energy of $E = 2.60$ eV. (All the TDTR time-delay data are shifted so the maximum change in the in-phase signal corresponds to $t = 0$; this time shift is used in the TR-MOKE data analysis later.) The TDTR data have distinct dynamics on timescales of picoseconds, hundreds of picoseconds, and nanoseconds. The initial rise in thermoreflectance from 0 to 1 ps is due to thermal transport by nonequilibrium electrons [5]. The subsequent decay from 1 to 3 ps is due to electron-phonon thermalization. Then, the thermoreflectance signal increases for ~500 ps as heat diffuses across the thick Au layer. On timescales longer than 0.5 ns, the thermoreflectance signal decays as heat diffuses out of the metal multilayer and into the sapphire substrate.

We use picosecond acoustic signals in our TDTR data to determine the Au film thickness in the region where the laser is focused on the sample. Pump heating of the Au/Co multilayer generates a longitudinal acoustic pulse. After traversing the Au layer, the acoustic pulse reaches the surface of the Au layer and modifies the reflectance of the Au film. For the region of the sample where the data in Fig. 2(b) was collected, the acoustic pulse takes ~61 ps to traverse the metal multilayer. The longitudinal speed of sound in Au is 3.45 nm/ps, corresponding to $d_{Au} \approx 210$ nm.

The primary aim of our study is to use the strength of TR-MOKE signal as a function of probe wavelength to determine the magneto-optical spectra of Au. However, the wavelength dependence of the optical spectra is not the only parameter that affects signal amplitude vs wavelength. TDTR signal amplitude also depends on the incident fluence of the pump beam, the absorbance of the sample, transmissivity of the objective lens, and the modulation amplitude of the pump beam by the electro-optical modulator. TR-MOKE signal depends on all of these factors, and also depends on the laser pulse duration. (By measuring the TR-MOKE signal amplitude scaled as a function of pump-pulse duration, we observed the signal strength is proportional to the inverse of the pulse duration.) Therefore, to facilitate comparison between our measurements at different wavelengths, we normalize the raw data to account for the wavelength dependence of the various

(b) Same experiment as in (a), but extended to nanosecond timescales and plotted on a log scale. The feature at 61 ps is due to a longitudinal strain wave. A 61-ps time of flight corresponds to a Au film thickness of 210 nm. The maximum in-phase voltage signal occurs at 500 ps, which is time required for the Au film to thermalize. (c) Thermoreflectance coefficient, dR/dT, vs photon energy measured for Au. The thermoreflectance coefficient values were derived from probe energy-dependent TDTR signals, like the ones shown in (a) and (b). Filled symbols correspond to positive thermoreflectance values. Open symbols correspond to negative values. The green line is experimental data for thermoreflectance spectra of Au from Wilson *et al.* [41].
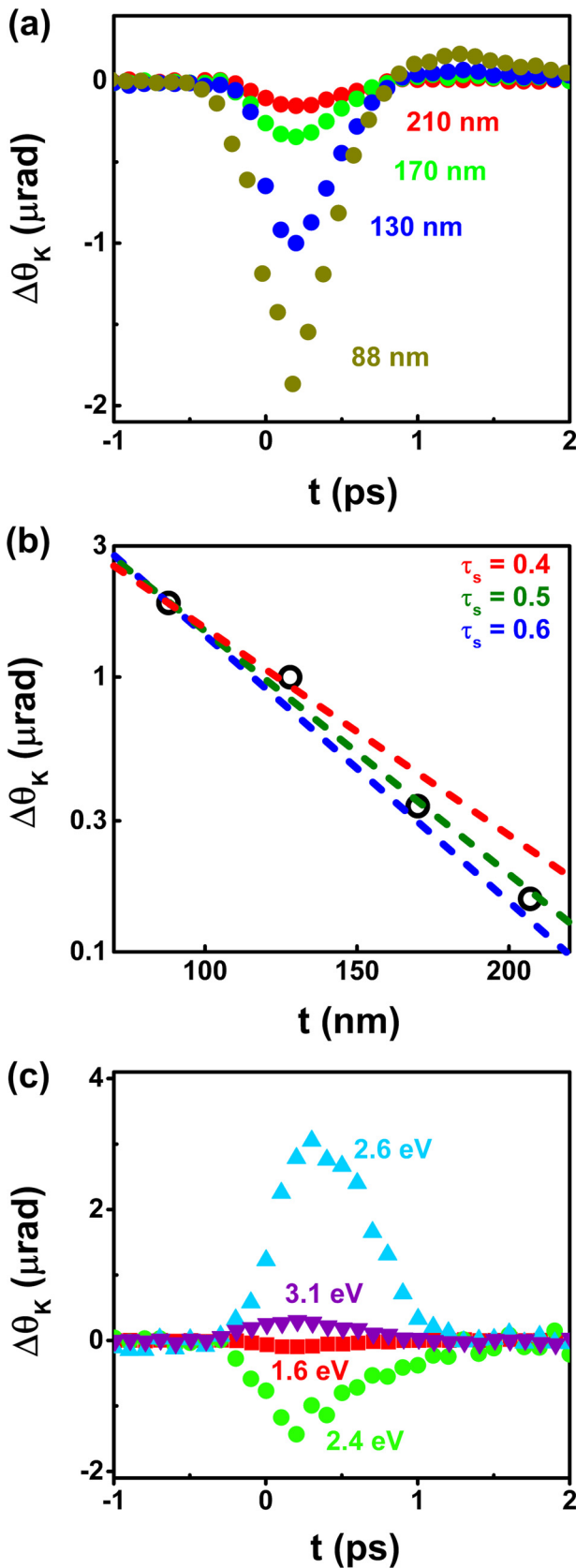
parameters described above. Specifically, these data are normalized to the signal that would be observed if the absorbed fluence was 4.4 J/m^2 and the laser pulse duration was 160 fs.

In Figs. 2 and 3, we report the normalized pump/probe data. The signals in a TDTR experiment (Fig. 2) depend on the temperature evolution of the sample in response to pump heating, and the thermoreflectance coefficient of the Au layer, dR/dT. The temperature response of metal multilayers in response to pulsed heating is well understood and can be accurately predicted with thermal models [40]. Therefore, by comparing thermal model predictions to experimental TDTR data [41], we can determine the thermoreflectance coefficient of Au vs wavelength from our TDTR measurements. In Fig. 2(c), we compare the energy dependence of the thermoreflectance coefficient determined from our experiments to prior measurements for Au thermoreflectance spectra. We followed the same analytical procedure as outlined in Wilson *et al.* [41], with minor modifications to account for differences in detection electronics for our pump/probe system [31]. The magnitude and energy dependence of dR/dT are in agreement with previously reported values [41,42].

We now turn our attention to the results of the TR-MOKE measurements. Before performing wavelength-dependent TR-MOKE studies, we conducted TR-MOKE measurements as a function of Au thickness. We did this to evaluate the experimental tradeoffs related to Au film thickness. In agreement with prior work by Choi *et al.* [5], we observe that the signal strength decreases with increasing Au thickness; see Fig. 3(a). The decrease in signal with increasing thickness is due to spin accumulation being distributed across a larger volume as the thickness of the gold layer increases, and the finite spin-diffusion length of Au. The thickness dependence of our MOKE signals is consistent with a Au spin-diffuion length of ~70 ± 10 nm [Fig. 3(b)]. The decrease in MOKE signal for increasing Au thicknesses is undesirable for our purposes. But, there are other advantages to a thick Au layer. For Au thicknesses not sufficiently thick, experimental signals become sensitive to the magneto-optical response of the buried Co layers [5]. Since our goal is to measure the MOKE of Au, we need to eliminate any contributions to our signal from Co. Another problem we observe when the Au film is too thin is leaked pump light. For experiments with a frequency-doubled probe beam, we use optical filters to prevent pump light from reaching the photodetector. However, when conducting experiments with a near-infrared probe, the probe and pump are the same energy, and so we cannot use an optical filter to prevent pump light from reaching the detector. After extensive trial and error, we discovered that a gold layer thickness of 200 nm was sufficient to prevent pump light from reaching the detector, and to remove any contribution to the MOKE signal from Co at all wavelengths. Consequently, we conducted all wavelength-dependent pump/probe measurements at a region of the sample where $d_{\text{Au}} \approx 210$ nm.

FIG. 3. Time-resolved magneto-optic Kerr effect experiments. (a) Kerr rotation vs pump/probe time delay for a photon energy $E = 1.70$ *e* for different Au film thicknesses; (b) dependence of the peak Kerr rotation vs film thickness; black circles correspond to experimental values. Dashed lines are from calculations done in Choi *et al.* [5]; and (c) Kerr rotation of Au vs pump/probe time delay for different photon energies.
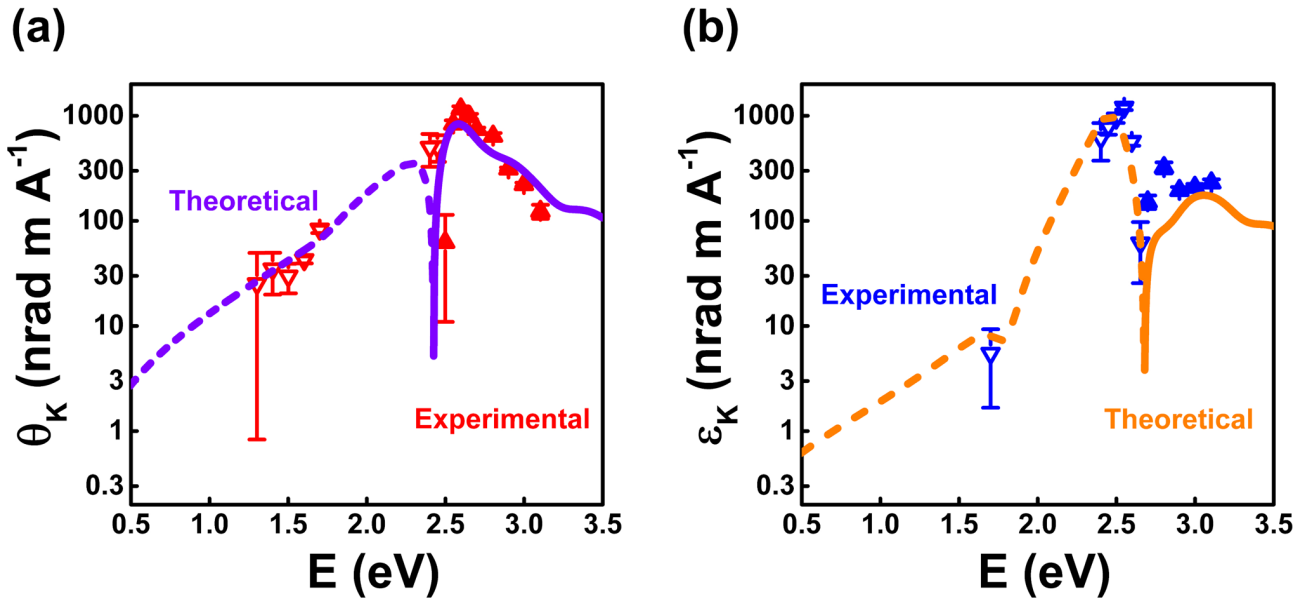
FIG. 4. Photon energy-dependent Kerr angles per magnetic moment for a Au film. (a) Kerr rotation and (b) Kerr ellipticity of Au. The magnetic moment is obtained by using the conversion factor obtained in Kimling *et al.* [11]. Filled symbols correspond to positive values, while open symbols correspond to negative values. Values below the floor noise level were omitted. The lines correspond to the theoretical predictions obtained by density-functional theory, solid lines correspond to positive values, and dashed lines correspond to negative values.

To determine the amount of spin accumulation in our samples, we use the previously reported value of 43 nrad per A/m measure for Au at 780 nm [11]. This value for the real Kerr angle of Au per magnetic moment was arrived at via careful comparison of two types of experiments [5,11]. The precessional dynamics in a spin-transfer torque multilayer were analyzed, and then compared to TR-MOKE data collected on a sample geometry similar to the one we study here. The data for the spin-transfer torque multilayer were analyzed with a spin-diffusion model and Landau-Lifshitz-Gilbert equation. The analysis related the amplitude of the precessional dynamics to the amount of spin current generated by the pump excitation [5,11]. We note that extracting the value of 43 nrad per A/m from these two experiments is not straightforward, and the accuracy of this value depends on the accuracy of the spin-diffusion model used in Ref. [11]. Kimling [11] estimated the uncertainty to be ∼30%. (Choi reports a value of ∼24 nrad per A/m [5], but follow-up work reported an experimental calibration error that led to a factor of 1.8 underestimation of the Kerr rotation [11].) With a value of 43 nrad per A/m at 780 nm (1.59 eV), we deduce that for an incident pump-absorbed fluence of 4.4 J/m^2, a laser pulse duration of 160 fs, and pump and probe wavelengths of 1.6 eV, the peak spin accumulation at the surface of the 210-nm Au layer is ≈2.6 A/m at a delay time of ∼0.5 ps.

The results of the TR-MOKE measurements as a function of probe energy are shown in Figs. 3 and 4. These data are the primary result of our study. We performed two TR-MOKE scans at each probe energy: one scan to measure the real Kerr angle of Au, and one scan to measure the imaginary Kerr angle. All together, we performed 32 experiments at 16 probe energies. We show TR-MOKE scans in Fig. 3(b) at probe energies of 1.6, 2.4, 2.6, and 3.1 eV. Figure 4 reports

the maximum of the transient Kerr signals as a function of probe energy. Figure 4(a) shows the real part of the Kerr angle (rotation), and Fig. 4(b) shows the imaginary part (ellipticity). In addition to the data points shown in Fig. 4, we performed several measurements at probe energies between 1.2 and 1.4 eV. However, the MOKE signal at these energies dropped below the noise-floor level of our experimental technique, so at energies between 1.2 and 1.4 eV, our experiments can only bound the real and imaginary Kerr angles to be less than 10 nrad per A/m.

We compare our experimental data to the results of the density-functional theory calculations in Fig. 4. DFT predicts the same spectral behavior that we observe experimentally, with maxima in the Kerr response of Au near the interband transition threshold energy of 2.5 eV. Consistent with our experimental observations, at near-infrared energies below 1.7 eV, DFT predicts a real Kerr angle ∼10× larger than the imaginary Kerr angle.

IV. DISCUSSION

The most striking result of our study is our observation that the Kerr spectra for Au has a sharp Lorentzian line shape like the kind associated with a high *Q*-factor oscillator. The Lorentzian is centered at the interband transition threshold of 2.5 eV with a large amplitude. The imaginary Kerr angle peaks near 2.5 eV at a value above ∼1 µrad per A/m. The real Kerr angle peaks near 2.6 eV at ∼1 µrad per A/m. Near the interband transition threshold, the Kerr response of Au is ∼20× larger than it is at near-infrared photon energies, e.g., the 1.6 eV where the vast majority of TR-MOKE experiments are conducted. For comparison, the Kerr angle of nickel has a maximum value of ≈4 mrad at a photon

energy of ≈ 4 eV [43]. Nickel has a magnetic moment of $\approx 5.1 \times 10^5$ A/m, so the Kerr angle per magnetization in Ni has a maximum of only 8 nrad per A/m, more than two orders of magnitude smaller than the maxima we observe for Au. The sensitivity of the optical properties of Au to spin accumulation is also much larger than DFT predictions for other nonmagnetic heavy metals. Stamm *et al.* report DFT predictions for the longitudinal MOKE spectra of Pt and W; using their calculated values gives that Pt has a maximum Kerr angle of 10 nrad per A/m at 4.1 eV, while W has a maximum Kerr angle of 13 nrad per A/m at 1.2 eV [10].

A careful decomposition of our DFT calculations allows us to determine that the complex Kerr spectra at energies between 1 and 4 eV is dominated by optical transitions between d states and s states. Intraband transitions do not play a significant role until lower energies, e.g., less than 100 meV. As a result, the Kerr response drops rapidly at energies below the d-to-s interband transition threshold of 2.5 eV. Qualitatively, the Lorentzian-like response can be understood by considering how two factors affect interband transitions. At the Fermi level, spin accumulation leads to a change in the occupation function for up vs down electrons, which alters the transition probabilities in Eq. (1). Spin-orbit splitting of the d bands also affects transition probabilities. Together, these effects lead to a large polarization-dependent index of refraction (Kerr rotation), and large polarization-dependent absorption (ellipticity) for photon energies near the interband transition threshold.

Even at energies well below the interband transition threshold of 2.5 eV, e.g., 1.5 eV, DFT predicts a significant Kerr rotation as a result of d- to s-state transition effects. Lifetime broadening means transition probabilities are nonzero even for photon energies below the interband transition threshold of 2.5 eV. At low energies, e.g., 1 to 1.5 eV, the effect of the transitions from d- to s states on the diagonal part of the optical conductivity tensor σ_{xy} is small compared to the Drude term [44]. However, this is not the case for the off-diagonal part of σ_{xy}, as the Drude term does not contribute to it. Therefore, the small off-diagonal part of σ_{xy} at low energies, e.g., 1 to 1.5 eV, in our calculations originates from the lifetime broadening of the d- to s-state transition.

Our density-functional theory calculations include effects of spin-orbit coupling on the band structure, but do not include effects from skew- or side-jump scattering, or surfaces. Our Au films are (111) textured, and spin-orbit interactions are known to cause $\approx 100-$meV splitting of the s-p bands near the Fermi-level at Au (111) surfaces [30]. Prior work has explained near-infrared MOKE measurements of nonmagnetic metals with skew-scattering theories [5,45]. The good agreement between theory and experiment in our study suggests surfaces, skew scattering, and side-jump scattering are probably not important processes for the MOKE spectra of Au at visible and near-infrared frequencies. Definitively determining the importance of surfaces and spin-dependent electronic scattering processes would require extending measurements to lower energies in the near infrared, e.g., less than 1 eV. At such low frequencies, our theory predicts that the effect of d-state to s-state transitions is negligible; see Fig. 4. Therefore, contributions from other effects would be easier to resolve at low energies.

Our work reports the effect of spin magnetic moments on magneto-optical spectra of Au. Prior experimental and theoretical work reports the magneto-optical spectra of noble metals in the presence of static magnetic fields [4]. In static-field experiments, three effects give rise to magneto-optical properties: the effect of Lorentz force on free-electron motion, orbital moments, and spin moments. We point out that the optical spectra in Au we observe from spin accumulation are different from the spectra observed due to static fields [4], especially in the near infrared. The differences in spectra for these related experiments suggest that wavelength-dependent measurements of MOKE could allow independent measurements of orbital vs spin moments in a metal. Separating spin and orbital contributions to magnetism would be useful for a variety of applications. One such application is inverse Faraday effect experiments, where circularly polarized light is believed to induce both orbital and spin moments [27].

Quantitative knowledge of the complex Kerr spectra of Au offers new opportunities for the design of optical experiments for characterizing spintronic devices. For example, low-noise green laser diodes are commercially available. MOKE systems built with such green lasers can use Au thin films as a transducer for the measurement of spin accumulation. Assuming a MOKE noise floor of ~ 100 nrad, a MOKE system with a green laser would have sensitivity to ~ 0.1 A/m, or ~ 2 spins per million atoms. Such sensitivity to small magnetic moments would enable experiments not otherwise possible [46]. Similarly, our results will aid in the design of optical experiments designed to study ultrafast magnetization dynamics of complex magnetic heterostructures. Prior studies have shown that separate measurements of both the real and imaginary Kerr signals allows independent determination of the time-dependent magnetization dynamics of as many as two layers [47,48]. Scanning wavelengths to adjust sensitivity to specific layers in a heterostructure may offer the opportunity for table-top optical MOKE systems to characterize dynamics in more complex multilayer structures, like what is possible with x-ray techniques [49].

V. CONCLUSION

We measured the magneto-optic response of gold due to spin accumulation for photon energies in the near-infrared (1.3–1.7 eV) and visible (2.4–3.1 eV) spectrum. We observed a sharp transition in the Kerr rotation as a consequence of the interband transition at $E = 2.50$ eV. Our results display a good agreement with the DFT theoretical model, suggesting that extrinsic scattering processes do not provide a significant contribution to the magneto-optic response in gold at energies between 1.3 and 3.1 eV. Instead, the Kerr response of Au appears to be dominated by optical transitions between the s bands and d bands. We find that for photon energies near 2.5 eV, Au is an extremely sensitive optical magnetometer. These results provide opportunities for the development of ultrasensitive optical spintronic devices.

The data that support the findings of this study are available from the corresponding author upon reasonable request [50].

[1] N. Nagaosa, J. Sinova, S. Onoda, A. H. MacDonald, and N. P. Ong, Anomalous Hall effect, Rev. Mod. Phys. **82**, 1539 (2010).

[2] P. N. Argyres, Theory of the Faraday and Kerr effects in ferromagnetics, Phys. Rev. **97**, 334 (1955).

[3] C. Kittel, *Introduction to Solid State Physics*, 8th ed. (John Wiley and Sons, New Jersey, 1947).

[4] L. Uba, S. Uba, and V. N. Antonov, Magneto-optical Kerr spectroscopy of noble metals, Phys. Rev. B **96**, 235132 (2017).

[5] G.-M. Choi and D. G. Cahill, Kerr rotation in Cu, Ag, and Au driven by spin accumulation and spin-orbit coupling, Phys. Rev. B **90**, 214432 (2014).

[6] L. Uba, S. Uba, V. N. Antonov, A. N. Yaresko, and R. Gontarz, Magneto-optical Kerr spectroscopy of platinum, Phys. Rev. B **62**, 16510 (2000).

[7] J. C. McGroddy, A. J. McAlister, and E. A. Stern, Polar reflection Faraday effect in silver and gold, Phys. Rev. **139**, A1844 (1965).

[8] C. A. Herreño-Fierro and E. J. Patiño, Maximization of surface-enhanced transversal magneto-optic Kerr effect in Au/Co/Au thin films, Phys. Status Solidi Basic Res. **252**, 316 (2015).

[9] A. Melnikov, I. Razdolski, T. O. Wehling, E. T. Papaioannou, V. Roddatis, P. Fumagalli, O. Aktsipetrov, A. I. Lichtenstein, and U. Bovensiepen, Ultrafast Transport of Laser-Excited Spin-Polarized Carriers in Au/Fe/MgO(001), Phys. Rev. Lett. **107**, 076601 (2011).

[10] C. Stamm, C. Murer, M. Berritta, J. Feng, M. Gabureac, P. M. Oppeneer, and P. Gambardella, Magneto-Optical Detection of the Spin Hall Effect in Pt and W Thin Films, Phys. Rev. Lett. **119**, 087203 (2017).

[11] J. Kimling and D. G. Cahill, Spin diffusion induced by pulsed-laser heating and the role of spin heat accumulation, Phys. Rev. B **95**, 014402 (2017).

[12] J. Kimling, G.-M. Choi, J. T. Brangham, T. Matalla-Wagner, T. Huebner, T. Kuschel, F. Yang, and D. G. Cahill, Picosecond Spin Seebeck Effect, Phys. Rev. Lett. **118**, 057201 (2017).

[13] V. H. Ortiz, M. J. Gomez, Y. Liu, M. Aldosary, J. Shi, and R. B. Wilson, Ultrafast measurements of the interfacial spin Seebeck effect in Au and rare-earth iron-garnet bilayers, Phys. Rev. Mater. **5**, 074401 (2021).

[14] M. Hofherr, P. Maldonado, O. Schmitt, M. Berritta, U. Bierbrauer, S. Sadashivaiah, A. J. Schellekens, B. Koopmans, D. Steil, M. Cinchetti, B. Stadtmüller, P. M. Oppeneer, S. Mathias, and M. Aeschlimann, Speed and efficiency of femtosecond spin current injection into a nonmagnetic material, Phys. Rev. B **96**, 100403 (2017).

[15] G. Armelles, A. Cebollada, A. García-Martín, and M. U. González, Magnetoplasmonics: Combining magnetic and plasmonic functionalities, Adv. Opt. Mater. **1**, 10 (2013).

[16] O. Kovalenko, M. Vomir, B. Donnio, J. L. Gallani, and M. V. Rastei, Chiromagnetoptics of Au and Ag nanoparticulate systems, J. Phys. Chem. C **124**, 21722 (2020).

[17] M. Moocarme, J. L. Domínguez-Juárez, and L. T. Vuong, Ultralow-intensity magneto-optical and mechanical effects in metal nanocolloids, Nano Lett. **14**, 1178 (2014).

[18] N. V. Proscia, M. Moocarme, R. Chang, I. Kretzschmar, V. M. Menon, and L. T. Vuong, Control of photo-induced voltages in plasmonic crystals via spin-orbit interactions, Opt. Express **24**, 10402 (2016).

[19] V. I. Belotelov, E. A. Bezus, L. L. Doskolovich, A. N. Kalish, and A. K. Zvezdin, Inverse Faraday effect in plasmonic heterostructures, J. Phys.: Conf. Ser. **200**, 092003 (2010).

[20] J. Hurst, P. M. Oppeneer, G. Manfredi, and P. A. Hervieux, Magnetic moment generation in small gold nanoparticles via the plasmonic inverse Faraday effect, Phys. Rev. B **98**, 134439 (2018).

[21] N. Maccaferri, I. Zubritskaya, I. Razdolski, I. A. Chioar, V. Belotelov, V. Kapaklis, P. M. Oppeneer, and A. Dmitriev, Nanoscale magnetophotonics, J. Appl. Phys. **127**, 080903 (2020).

[22] O. H. C. Cheng, D. H. Son, and M. Sheldon, Light-induced magnetism in plasmonic gold nanoparticles, Nat. Photon. **14**, 365 (2020).

[23] R. Sinha-Roy, J. Hurst, G. Manfredi, and P. A. Hervieux, Driving orbital magnetism in metallic nanoparticles through circularly polarized light: A real-time TDDFT study, ACS Photon. **7**, 2429 (2020).

[24] R. Hertel, Theory of the inverse Faraday effect in metals, J. Magn. Magn. Mater. **303**, L1 (2006).

[25] J. P. Van Der Ziel, P. S. Pershan, and L. D. Malmstrom, Optically-Induced Magnetization Resulting from the Inverse Faraday Effect, Phys. Rev. Lett. **15**, 190 (1965).

[26] M. Battiato, G. Barbalinardo, and P. M. Oppeneer, Quantum theory of the inverse Faraday effect, Phys. Rev. B **89**, 014413 (2014).

[27] M. Berritta, R. Mondal, K. Carva, and P. M. Oppeneer, Ab Initio Theory of Coherent Laser-Induced Magnetization in Metals, Phys. Rev. Lett. **117**, 137203 (2016).

[28] K. H. J. Buschow, P. G. van Engen, and R. Jongebreur, Magneto-optical properties of metallic ferromagnetic materials, J. Magn. Magn. Mater. **38**, 1 (1983).

[29] T. Higo, H. Man, D. B. Gopman, L. Wu, T. Koretsune, O. M. J. Van 'T Erve, Y. P. Kabanov, D. Rees, Y. Li, M. T. Suzuki, S. Patankar, M. Ikhlas, C. L. Chien, R. Arita, R. D. Shull, J. Orenstein, and S. Nakatsuji, Large magneto-optical Kerr effect and imaging of magnetic octupole domains in an antiferromagnetic metal, Nat. Photon. **12**, 73 (2018).

[30] S. LaShell, B. A. McDougall, and E. Jensen, Spin Splitting of a Au(111) Surface State Band Observed with Angle Resolved Photoelectron Spectroscopy, Phys. Rev. Lett. **77**, 3419 (1996).

[31] M. J. Gomez, K. Liu, J. G. Lee, and R. B. Wilson, High sensitivity pump–probe measurements of magnetic, thermal, and acoustic phenomena with a spectrally tunable oscillator, Rev. Sci. Instrum. **91**, 023905 (2020).

[32] N. Wiser, Dielectric constant with local field effects included, Phys. Rev. **129**, 62 (1963).

[33] S. L. Adler, Quantum theory of the dielectric constant in real solids, Phys. Rev. **126**, 413 (1962).

[34] K. Liu, X. Shi, R. Mohan, J. Gorchon, S. Coh, R. B. Wilson, F. Angeles, R. Mohan, J. Gorchon, S. Coh, and R. B. Wilson, Differentiating contributions of electrons and phonons to the thermoreflectance spectra of gold, Phys. Rev. Mater. **5**, 106001 (2021).

[35] See Supplemental Material at http://link.aps.org/supplemental/10.1103/PhysRevB.106.014410 for more information about the effects of extrinsic scattering to the conductivity tensor.

[36] P. Giannozzi, O. Baseggio, P. Bonfà, D. Brunato, R. Car, I. Carnimeo, C. Cavazzoni, S. de Gironcoli, P. Delugas, F. Ferrari Ruffino, A. Ferretti, N. Marzari, I. Timrov, A. Urru, and S. Baroni, Quantum ESPRESSO toward the exascale, J. Chem. Phys. **152**, 154105 (2020).

[37] A. M. Brown, R. Sundararaman, P. Narang, W. A. Goddard, and H. A. Atwater, Ab initio phonon coupling and optical response of hot electrons in plasmonic metals, Phys. Rev. B **94**, 075120 (2016).

[38] C. Rizal and E. E. Fullerton, Perpendicular magnetic anisotropy and microstructure properties of nanoscale Co/Au multilayers, J. Phys. D: Appl. Phys. **50**, 355002 (2017).

[39] G. M. Choi, B. C. Min, K. J. Lee, and D. G. Cahill, Spin current generated by thermally driven ultrafast demagnetization, Nat. Commun. **5**, 4334 (2014).

[40] D. G. Cahill, Analysis of heat flow in layered structures for time-domain thermoreflectance, Rev. Sci. Instrum. **75**, 5119 (2004).

[41] R. B. Wilson, B. A. Apgar, L. W. Martin, and D. G. Cahill, Thermoreflectance of metal transducers for optical pump-probe studies of thermal properties, Opt. Express **20**, 28829 (2012).

[42] W. J. Scouler, Temperature-Modulated Reflectance of Gold from 2 to 10 eV, Phys. Rev. Lett. **18**, 445 (1967).

[43] P. M. Oppeneer, T. Maurer, J. Sticht, and J. Kübler, Ab initio calculated magneto-optical Kerr effect of ferromagnetic Metals: Fe and Ni, Phys. Rev. B **45**, 10924 (1992).

[44] See Supplemental Material at http://link.aps.org/supplemental/10.1103/PhysRevB.106.014410 for more information about the effects of extrinsic scattering to theoretical Kerr angles.

[45] A. Alekhin, I. Razdolski, M. Berritta, D. Bürstel, V. Temnov, D. Diesing, U. Bovensiepen, G. Woltersdorf, P. M. Oppeneer, and A. Melnikov, Magneto-optical properties of Au upon the injection of hot spin-polarized electrons across Fe/Au(0 0 1) interfaces, J. Phys.: Condens. Matter **31**, 124002 (2019).

[46] Y. Su, H. Wang, J. Li, C. Tian, R. Wu, X. Jin, and Y. R. Shen, Absence of detectable MOKE signals from spin Hall effect in metals, Appl. Phys. Lett. **110**, 042401 (2017).

[47] A. J. Schellekens, N. de Vries, J. Lucassen, and B. Koopmans, Exploring laser-induced interlayer spin transfer by an all-optical method, Phys. Rev. B **90**, 104429 (2014).

[48] J. Gorchon, C. H. Lambert, Y. Yang, A. Pattabi, R. B. Wilson, S. Salahuddin, and J. Bokor, Single shot ultrafast all optical magnetization switching of ferromagnetic Co/Pt multilayers, Appl. Phys. Lett. **111**, 042401 (2017).

[49] R. Kukreja, S. Bonetti, Z. Chen, D. Backes, Y. Acremann, J. A. Katine, A. D. Kent, H. A. Dürr, H. Ohldag, and J. Stöhr, X-Ray Detection of Transient Magnetic Moments Induced by a Spin Current in Cu, Phys. Rev. Lett. **115**, 096601 (2015).

[50] For experimental data request, please contact the corresponding author (rwilson@ucr.edu).

Correction: A byline footnote has been added for the second author.